Incorporation of Nanoparticles into Polymersomes: Size and Concentration Effects

Karmena Jaskiewicz,[†] Antje Larsen,[‡] David Schaeffel,[†] Kaloian Koynov,[†] Ingo Lieberwirth,[†] George Fytas,[†,‡] Katharina Landfester,[†] and Anja Kroeger[†,*]

[†]Max Planck Institute for Polymer Research, Ackermannweg 10, 55128 Mainz, Germany and [‡]Department of Materials Science and Technology, University of Crete and F.O.R.T.H., P.O. Box 1527, 71110 Heraklion, Greece

ABSTRACT

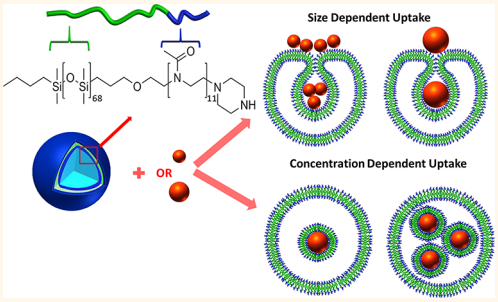

Because of the rapidly growing field of nanoparticles in therapeutic applications, understanding and controlling the interaction between nanoparticles and membranes is of great importance. While a membrane is exposed to nanoparticles its behavior is mediated by both their biological and physical properties. Constant interplay of these biological and physicochemical factors makes selective studies of nanoparticles uptake demanding. Artificial model membranes can serve as a platform to investigate physical parameters of the process in the absence of any biofunctional molecules and/or supplementary energy. Here we report on photon- and fluorescence-correlation spectroscopic studies of the uptake of nanosized SiO_2 nanoparticles by poly(dimethylsiloxane)-*block*-poly(2-methyloxazoline) vesicles allowing species selectivity. Analogous to the cell membrane, polymeric membrane incorporates particles using membrane fission and particles wrapping as suggested by cryo-TEM imaging. It is revealed that the incorporation process can be controlled to a significant extent by changing nanoparticles size and concentration. Conditions for nanoparticle uptake and controlled filling of polymersomes are presented.

KEYWORDS: nanoparticles · transport · model membrane · vesicles · photon correlation spectroscopy · fluorescence correlation spectroscopy

The high complexity of native natural membranes and the diverse coupling of interactions within these bilayer structures have inspired the development of simplified model systems.[1,2] A wide variety of approaches including free-standing[1,3,4] and tethered vesicles[1,5] as well as solid-supported and planar bilayers[6−8] provide various experimental platforms to study systematically the physical and chemical characteristics of individual membrane components, their interplay, and different aspects of structure−property relations as well as the role of interactions with the environment.[9−12] However, functional aspects, for example, the transmembrane transport, are barely accessible to these model systems. In particular, one of the most important functions of a living cell is the selective transport of ions, molecules, or colloidal particles across the hydrophobic bilayer from the extracellular environment to the cell interior mediated by different endocytic machineries.[13] Mechano-chemistry of such coordinated processes fascinated scientists for over a century, but we are still far from a comprehensive description.[14,15] The mechanisms behind endocytosis are an object of intensive theoretical simulations,[16−23] while experimental studies are very limited.[24,25]

The key stage in endocytic processes is the adherence of a particle on the membrane, followed by an invagination of the fluid bilayer and complete wrapping of the target. Subsequently, the membrane-coated particle is detached from the outer membrane.[13] The growing field of engineered nanosized particles for biomedical application,[26,27] which are mainly uptaken utilizing endocytic pathways, is still intuitive due to the lack of detailed understanding of the incorporation mechanisms.[28,29] Whereas in biology endocytosis is a result of a complex interplay between membrane physical properties assisted by biofunctional molecules and/or supplementary energy, recent studies have revealed the existence of nonendocytotic incorporation mechanisms for nanoscaled objects.[30−33] Decoupling of these mutual interactions is only possible inside artificial membranes where one can focus on physical aspects while

* Address correspondence to kroeger@mpip-mainz.mpg.de.

Received for review May 29, 2012 and accepted July 16, 2012.

Published online July 16, 2012
10.1021/nn302367m

© 2012 American Chemical Society

biochemical processes are missing. Therefore, we developed a minimal model system based on amphiphilic block copolymer vesicles moving freely in solution, which allows the uncoupling of all involved interactions and processes.[25] Requirements for this purpose are long-term stability, and subtle balance between rigidity and elasticity of the model membrane.[34] Phospholipids, the natural constitutive units of membranes, which spontaneously form liposomes[35,36] when certain lipids are dispersed in aqueous medium, are mostly used as building blocks in the aforementioned approaches.[1−8] The major drawbacks of lipid membranes are the long-term instability and the limited chemical stability caused by oxidation processes of unsaturated fatty acids and the hydrolysis of ester bonds.[34] One promising alternative are amphiphilic block copolymers, which also self-assemble under certain conditions into vesicles (polymersomes).[9]

Both polymersome and liposome properties are strongly influenced by the characteristics of amphiphilic molecules.[37−39] In contrast to liposomes where lipid properties manipulation is limited, the thickness, bending and stretching moduli, and the permeability of the polymeric membrane can be easily tuned by changing the block copolymer molecular characteristics. Polymer molecular mass, polydispersity, and the structure of building blocks are the key parameters responsible for the polymeric bilayer performance.[37,38,40] A library of amphiphilic molecules which are able to self-assemble into vesicular structures[41,42] has expanded due to the progress in living polymerization methods opening new ways to manipulate the features of the polymersomes.

We have recently reported on the experimental observation of transmembrane transport of spherical polystyrene (PS) as well as silica (SiO_2) nanoparticles (NPs) into polymeric vesicles *via* an internalization process.[25] Here, curvature-mediated attractive interactions (strong adhesion) between NPs and polymersomes triggered membrane deformation and subsequent fission of the bilayer.[19,22,25] In this case of the absence of biofunctional molecules and/or supplementary energy, the process can involve four steps: (i) NP adsorption at the vesicle surface, (ii) engulfing of NPs by wrapping and the formation of necks, (iii) entire coverage of NPs by the membrane, and (iv) complete internalization of NPs. This particular identification is based on a single size and ratio of the geometric radii of the NPs to the polymersomes at a constant concentration.

On the theoretical side a balance between fluidity of the artificial membrane and short-ranged adhesive potential, given by a crucial size ratio is necessary for a successful incorporation process. In addition, the NP size should play an important role since the existence of a threshold particle size,[23] below which single NPs could not be internalized by a flexible membrane, has been proposed[19−22] and observed in cellular systems.[43−48] Nanoparticles below a certain size are simply not able to reduce the curvature energy of the membrane which is necessary for the nanoparticle engulfment. Therefore, the motivation for this work is 2-fold: to examine the size and concentration-dependent incorporation of spherical SiO_2 nanoparticles by polymeric model membranes and to determine conditions for NP uptake thereby creating the missing phenomenology. The variation of the NP mutual separation *via* change of particle concentration can help understanding the origin of different mechanisms of the incorporation process. For a selective probing of the dynamics of both interacting species we have combined photon (PCS) and fluorescence correlation (FCS) spectroscopy complemented by cryogenic transmission electron microscopy (cryo-TEM). From a detailed understanding of the complex interactions of NPs with polymeric model membranes benefits to the cellular particle uptake are anticipated.

RESULTS AND DISCUSSION

To investigate the size and concentration-dependent incorporation of SiO_2 NPs performed by poly(dimethylsiloxane)-*block*-poly(2-methyloxazoline) (PDMS-*b*-PMOXA) polymersomes (with a *z*-average hydrodynamic radius R_{hP} = 110 ± 3 nm), a dilute aqueous vesicle solution with a polymer concentration of $c_P = 4.5 \times 10^{-2}$ g L^{-1} was mixed with four different sizes of SiO_2 NPs ($R_{h\ NP}$ = (14 ± 1), (25 ± 2), (36 ± 2), and (57 ± 2) nm) at four different nanoparticle concentrations (c_{NP} = 0.05, 0.1, 0.15, and 0.2 g L^{-1}). Hence, the molar ratio of SiO_2 NPs to polymersomes ranges between 1300:1 and 4:1. These systems were characterized using PCS, FCS, and cryo-TEM allowing species selectivity. Because of the large optical contrast between water, polymersomes, and SiO_2 NPs the application of PCS to study the influences of different NP sizes and concentrations on the internalization process is optimal. The inner and outer refractive index of polymersomes formed in aqueous media ($n_{IN} = n_0$) are equal to that of water (n_{H_2O} = 1.333). Refractive index changes in the interior of the polymersomes (n_{IN}) caused by an internalization of SiO_2 NPs with n_{SiO_2} = 1.45, which is different from that of pure water, result in strongly altered total light scattering intensity $R_{vv}(q)$ of the investigated samples. Further, the combination of the large optical contrast and a core−shell architecture of the polymersomes will render both the form factor $P(q)$ and the scattering wave vector q dependence on the translational diffusion coefficient $D(q)$.[25]

Threshold Concentration. The influence of the NP size on the experimental $R_{vv}(q)$ as a function of q at a constant nanoparticle concentration of c_{NP} = 0.2 g L^{-1} is depicted in Figure 1; the molar ratio of SiO_2 NPs to polymersomes in these experiments ranges from

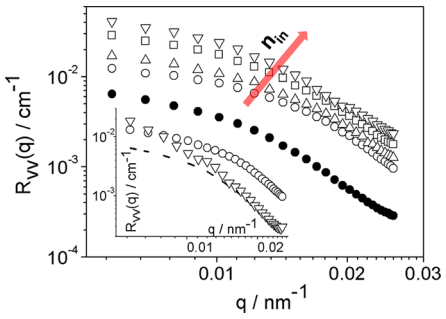

Figure 1. Absolute Rayleigh intensity $R_{vv}(q)$ as a function of the scattering wave vector q at $T = 20$ °C for polymersomes in the absence (solid circles) and in the presence of SiO_2 nanoparticles with different sizes; $R_{h\ NP} = 14$ nm (circles), 25 nm (triangles), 36 nm (squares), and 57 nm (inverse triangles) at $c_{NP} = 0.2$ g L^{-1} and $c_P = 4.5 \times 10^{-2}$ g L^{-1}. Inset: $R_{vv}(q)$ as a function q at $T = 20$ °C for the SiO_2/polymersomes systems with $R_{h\ NP} = 14$ nm (circles) and $R_{h\ NP} = 57$ nm (inverse triangles) at $c_P = 4.5 \times 10^{-2}$ g L^{-1} and $c_{NP} = 0.1$ g L^{-1}; the dashed line represents polymersomes in the absence of NPs.

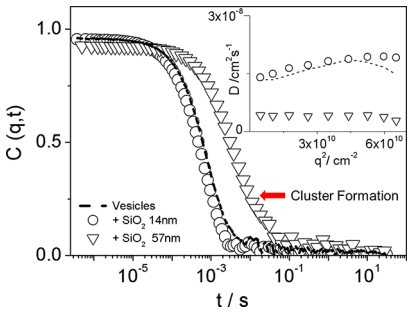

Figure 2. Relaxation functions $C(q, t)$ for the concentration fluctuations in SiO_2/polymersomes systems with $R_{h\ NP} = 14$ nm (circles) and 57 nm (inverse triangles) at $c_{NP} = 0.1$ g L^{-1} and $c_P = 4.5 \times 10^{-2}$ g L^{-1} for $q = 2.4 \times 10^{-2}$ nm^{-1} at $T = 20$ °C along with the translational diffusion $D(q)$ *vs* q^2 shown in the inset. The dashed lines represent polymersomes in the absence of NPs and the arrow points at the $C(q, t)$ yielding the slow translational diffusion (inverse triangles) of big clusters.

1260:1 for the smallest ($R_{h\ NP} = 14$ nm) to 16:1 for the largest NPs ($R_{h\ NP} = 57$ nm). The light scattering intensity for all NP containing samples is much higher than the sum of the individual component contributions (see Figure S1 in Supporting Information), indicating strong interactions of NPs with polymersomes. In comparison to the scattering intensity of solutions containing polymeric vesicles in the absence of NPs called, empty vesicles, $R_{vv}(q)$ values of SiO_2/polymersome samples increase with increasing NP sizes. The overall sizes of the resulting objects remain almost constant as indicated by the similar shape of the $R_{vv}(q)$ patterns. Since the contribution of the silica NPs to the total scattering intensity at low q values is negligible (see Figure S1 in Supporting Information), the observed increase of the forward scattering $R_{vv}(q \rightarrow 0)$ is associated to increasing values of n_{IN} due to NP internalization into the interior of the polymersomes as illustrated by the red arrow in Figure 1. This is fortuitous because the z-average hydrodynamic radius R_{hP} and the size polydispersity of the SiO_2/polymersome systems reveal only moderate changes.[49] In fact the pattern of $D(q)$ (see Figure 2 and Figure 5 below) obtained from the experimental concentration relaxation functions $C(q, t)$ in PCS experiments indicates no significant change in the value of R_{hP} and polydispersity (PDI) compared to the solutions containing empty vesicles. Therefore, mainly the increase of n_{IN}, relative to that of pure water, boosts the intensity $R_{vv}(q \rightarrow 0)$ as confirmed by fit model calculations of $P(q)$ with increasing n_{IN} (described later).

The inset of Figure 1 presents the increase of $R_{vv}(q)$ for the SiO_2 ($R_{h\ NP} = 14$ nm)/polymersomes system at $c_{NP} = 0.1$ g L^{-1} while the intensity pattern of the polymersome solution with large SiO_2 NPs ($R_{h\ NP} = 57$ nm) at the same c_{NP} reveals a different shape, which implies scattering from larger moieties. This notion is corroborated by the relaxation function $C(q, t)$ of Figure 2 displaying a single translational diffusion $D(q)$ (inverse triangles) which is significantly slower than both empty polymersomes and vesicles occupied by the small silica particles. The experimental $C(q, t)$ were represented by a stretched exponential function (see Methods for details) with a shape parameter (eq 1) $\beta_{KWW} = 0.95$ and $D(q) = \Gamma(q)/q^2$ (see inset in Figure 2 obtained from the relaxation rate $\Gamma(q)$. Hence the size of the diffusing objects increases significantly in case of SiO_2 ($R_{h\ NP} = 57$ nm)/polymersomes with $c_{NP} = 0.1$ g L^{-1} due to cluster formation. A decrease of c_{NP} down to 0.05 g L^{-1} causes agglomeration in the SiO_2/polymersome mixture not only with $R_{h\ NP} = 57$ nm but also with $R_{h\ NP} = 36$ nm (not shown) at SiO_2/polymersomes ratio 4:1 and 16:1, respectively.

This pertinent observation suggests the existence of a threshold particle concentration above which particle incorporation can occur. Such a threshold concentration is probably related to the surface area ratio between polymersomes and NPs[50] necessary for a successful particle adhesion to the outer vesicle membrane and further internalization. Changing c_{NP} results in the variation of the overall nanoparticles surface area (single nanoparticle surface area is constant). Estimation of the surface area ratio between polymersomes and NPs suggests to the conclusion that the overall surface area of the latter should be at least two times higher (see Table S1 in Supporting Information). For the two smallest NP sizes ($R_{h\ NP} = 14$ and 25 nm), the calculated threshold particle concentration should be less than the lowest investigated concentration of $c_{NP} = 0.05$ g L^{-1}; rough estimates amount to 0.025 g L^{-1} and 0.04 g L^{-1}, respectively.

Concentration Dependence. Figure 3 shows the experimental total light scattering intensity $R_{vv}(q)$ as a function of the scattering wave vector q for a SiO_2

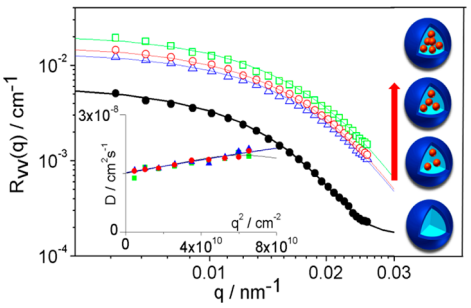

Figure 3. Absolute Rayleigh intensity $R_{vv}(q)$ pattern at T = 20 °C for polymersomes in the absence of NPs (solid black circles) and the SiO_2 ($R_{h\ NP}$ = 14 nm)/polymersome system at three different NP concentrations; c_{NP} = 0.1 g L^{-1} (blue triangles), 0.15 g L^{-1} (red circles), 0.2 g L^{-1} (green squares) represented by the corresponding theoretical expressions (solid lines), (see eq. S1 in Supporting Information). The increasing nanoparticle population inside the polymersomes with c_{NP} is schematically shown for the four systems. The inset depicts the corresponding translational diffusion coefficients $D(q)$ *vs* q^2 for the three different SiO_2/polymersome systems (solid symbols) and polymersomes in the absence of NPs (black line).

($R_{h\ NP}$ = 14 nm) /polymersome system at three different NP concentrations at a constant polymer concentration. The forward scattering intensity $R_{vv}(q \rightarrow 0)$ increases with c_{NP} while the scattering $R_{vv}(q)$ patterns are similar and distinct from the empty polymersomes (at high q-values). The increase of the refractive index in the interior of polymersomes n_{IN} (above the value of water) as a result of particle incorporation is the main parameter accounting for the forward scattering provided that the polymersome size remains insensitive to c_{NP}. A concurrent representation of the $R_{vv}(q)$ pattern intensity and the translational diffusion $D(q)$ is obtained by the corresponding theoretical expressions[25] (see Supporting Information) and calculated values of the polymersome radius, R_n, apparent weight-average molar mass, $M_{w\ app}$, of the objects, system polydispersity, PDI, and n_{IN} are listed in Table 1. Assuming a linear dependence of $n_{IN}(\phi)$ on particle volume fraction (in the interior of a polymersome) ϕ, the number x of incorporated nanoparticles increases from about 7 at c_{NP} = 0.1 g L^{-1} to 11 for c_{NP} = 0.2 g L^{-1} in the initial solution. Note that maximum filling of the particular polymersomes with SiO_2 ($R_{h\ NP}$ = 14 nm) would correspond to x = 43 incorporated particles assuming individual incorporation of particles; calculations based on group incorporation would lead to a higher number of incorporated particles (see Figure 6 below). In fact, cryo-TEM imaging[25] (Figure 6) and recent simulations[21] suggest incorporation of clusters of individual particles in some cases; PCS cannot distinguish between the two cases.

The incorporation of the particles is associated with shrinking of the polymersomes as indicated by the value of their radii listed in Table 1. To engulf and encapsulate nanoparticles membrane material is consumed.[24] The observed shrinking of about 18% is less than the estimated value of 24%, on the basis of the average number of the incorporated nanoparticles. This deviation can be partially attributed to the polydispersity (PDI in Table 1), not uniform filling, and probably bilayer stretching/vesicle swelling.[51] Internalization of the small SiO_2 beads occurs above 0.05 g L^{-1}, and their incorporation by the present polymersomes depends on the nanoparticle concentration in the bulk solution. Particles with $R_{h\ NP}$ = 25 nm retain this internalization behavior (see Table S2 in Supporting Information).

TABLE 1. Characteristics of Polymersomes in the Absence and Presence of SiO_2 NPs with $R_{h\ NP}$ = 15 nm

	polymersomes	SiO_2/polymersomes		
c_{NP} (g L^{-1})	0	0.1	0.15	0.2
$R_{vv}(q \rightarrow 0) \times 10^3$ (cm^{-1})	6.35	14.24	11.64	21.6
$M_{w\ app} \times 10^{-9}$ (g mol^{-1})	3.3	1.7	1.8	1.8
R_n (nm)	110	87	89	89
PDI	1.07	1.13	1.13	1.13
n_{IN}	1.333	1.367	1.373	1.382
x	0	7	9	11

Size Dependence. For the SiO_2/polymersome systems, samples with nanoparticle sizes of $R_{h\ NP}$ = 36 and 57 nm were prepared; interactions are observed above the threshold particle concentrations c_{NP} > 0.05 and 0.1 g L^{-1}, respectively. Above these critical concentrations, the mixtures exhibit $R_{vv}(q)$ beyond the sum of the individual components contributions (as described above). A peculiarity of these larger particles, however, is the strong contribution to $R_{vv}(q)$ at high q values and consequently to the relaxation function $C(q, t)$. For the investigation of the particle incorporation of these systems, both contributions should be properly accounted in order to enable an unambiguous discrimination between filled (NPs incorporated) *versus* decorated vesicles (NPs attached to outer polymersome surface).[25] An independent information on nanoparticles internalization would therefore facilitate the analysis of $R_{vv}(q)$ and $D(q)$ of the PCS experiment.

Fluorescence correlation spectroscopy is utilized by fluorescent labeling both interacting species, SiO_2 NPs ($R_{h\ NP}$ = 57 nm) and polymersomes. In a FCS experiment, the intensity fluctuations caused by the tracer diffusion of the fluorescent species through the focus of a confocal microscope are monitored and recorded. The correlation analysis of these fluctuations can yield information on both the size (R_h) and the concentration of the labeled species from the decay of the autocorrelation curve (diffusion time) and its plateau value at short lag times, respectively. Yet, labeling polymersomes and SiO_2 NPs with different fluorescent dyes and using two excitation lasers and appropriate emission filters (see Methods for details) permits selective probing through the utilization of the two FCS detection channels. The "blue" channel monitors only

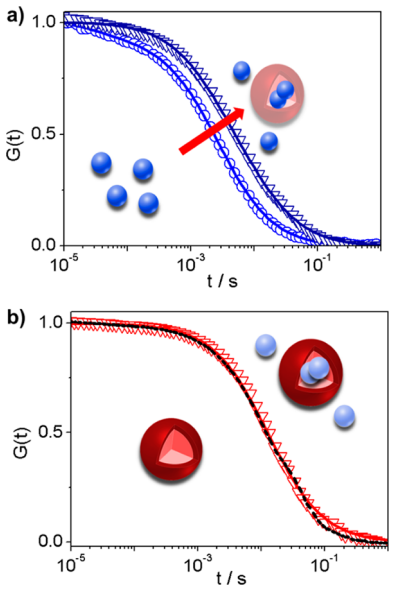

Figure 4. Normalized fluorescence intensity autocorrelation functions $G(t)$ for (a) distinctly labeled SiO_2 nanoparticles with $R_{hNP} = 57$ nm (blue symbols) and (b) polymersomes (red symbols) recorded before (circles in panel a and dotted black line in panel b) and after their mixing (inverse triangles). Solid lines in panel a represent fits of eq 2 to the experimental $G(t)$ assuming either a single diffusion ($i = 1$) before mixing or a double diffusion ($i = 2$) after mixing, whereas the solid red line in panel b denotes a single diffusion ($i = 1$) fit to the $G(t)$ (inverse triangles) for the SiO_2/labeled polymersome solution and the dotted black line represents $G(t)$ of empty vesicles.

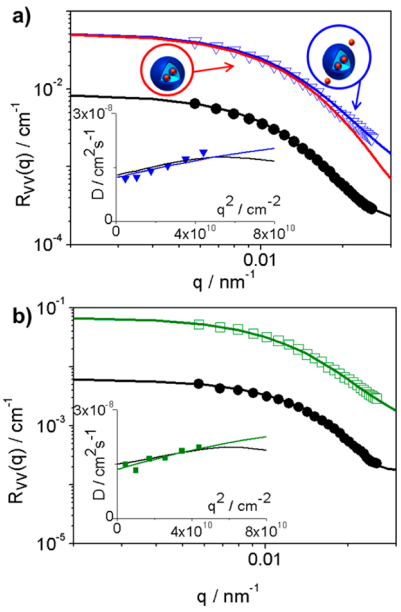

Figure 5. Absolute Rayleigh intensity $R_{vv}(q)$ at $T = 20$ °C of polymersomes in the absence of NPs (solid black circles) and the SiO_2/polymersome systems with (a) $R_{h\ NP} = 57$ nm (inverse triangles) and (b) $R_{h\ NP} = 36$ nm (squares) at $c_{NP} = 0.2$ g L^{-1} represented by the corresponding theoretical expressions (solid lines) along with the corresponding translational diffusion coefficient $D(q)$ *vs* q^2 (insets). The red line in panel a denotes the contribution of the filled polymersomes only (left scheme), whereas the total $R_{vv}(q)$ includes also the scattering from the free NPs (blue line) as shown in the right scheme of the figure. For the details of PCS data evaluation see the Supporting Information.

the fluorescent signal originating from the labeled SiO_2 NPs while the "red" channel detects the signal from the labeled polymersomes. Figure 4 presents fluorescence intensity autocorrelation curves $G(t)$ recorded in both channels before (circles) and after (inverse triangles) mixing polymersomes with SiO_2 beads at $c_P = 4.5 \cdot 10^{-2}$ gL^{-1} and $c_{NP} = 0.2$ g L^{-1}. As can be seen in Figure 4b, the correlation function for the polymersomes diffusion practically does not change upon mixing indicating either the absence of interactions or particle incorporation into the polymersomes. Indeed, if the nanoparticles were attached to the surface or trapped in the hydrophobic bilayer their relatively large size would cause a change in the overall diffusion coefficient of the polymersomes and therefore shift the decay of $G(t)$ to longer times. In the absence of such shift, the $G(t)$ recorded in the "red" channel for labeled polymersomes both with (inverse triangles) and without (solid red line in Figure 4b) nanoparticles can be fitted with eq 2 yielding $R_{hP} = 145 \pm 15$ nm for the polymersome hydrodynamic radius. At a first sight, the insensitivity of $G(t)$ to the presence of SiO_2 suggests robust polymersomes of average size.

Complementary information on the polymersome/NPs interactions is obtained from the fluorescence correlation function $G(t)$ of the labeled SiO_2 NPs seen in the "blue" FCS channel. Prior to their mixing with the polymersomes, $G(t)$ is well represented by a single diffusive decay in eq 2 (with $i = 1$) yielding $R_{h\ NP} = 55 \pm 5$ nm for the SiO_2 NPs in agreement with the PCS experiment. After mixing with the polymersomes, the experimental $G(t)$ shifts significantly toward longer lag times (blue inverse triangles) and deviates from a single diffusion in eq 2, instead, $G(t)$ is well represented eq 2 assuming two diffusive decays ($i = 2$). The first fast decay represents the freely diffusing, noninteracting SiO_2 beads, whereas the slow decay corresponds to the diffusion of much slower species with $R_h = 155 \pm 25$ nm being very close to the value for the polymersomes. Since only labeled SiO_2 NPs are probed, the slow process in $G(t)$ demonstrates internalization of the large SiO_2 particles ($R_{h\ NP} = 57$ nm). Yet the relative contribution of the slow decay, normalized to the inherent fluorescence intensities of the pure labeled solutions (SiO_2 NPs and polymersomes, see Methods) confirms this particle incorporation amounting to about two SiO_2 NPs per polymersome.

We turn now to the PCS information on large particle internalization addressed in Figure 5. Both $R_{vv}(q)$ and $D(q)$ patterns for SiO_2 ($R_{h\ NP} = 57$ nm)/polymersomes are well represented for an incorporation ratio 2:1 (red solid line) including the contribution of free particles in solution (blue solid lines) as schematically shown in Figure 5a. The necessity of a two component fit to $R_{vv}(q)$ and $D(q)$ is also implied by the

TABLE 2. Characteristics of Polymersomes in the Absence and Presence of SiO_2 NPs with $R_{h\ NP}$ = 36 and 57 nm

	SiO_2/polymersomes	
$R_{h\ NP}$ (nm)	36	57
c_{NP} (g L^{-1})	0.2	0.2
$R_{vv}(q \rightarrow 0) \times 10^3$ (cm^{-1})	44.7	83.2
$M_{w\ app} \times 10^{-9}$ ($gmol^{-1}$)	2.0	3.1
R_n (nm)	93	100
PDI	1.2	1.17
n_{IN}	1.396	1.417
x	3—4	2—3

fast diffusion at the highest q values (not included in the inset to Figure 5a) due the contribution of the free SiO_2 NPs to the scattering event. For comparison, Figure 5b shows the experimental $R_{vv}(q)$ and $D(q)$ for the same SiO_2/polymersomes system with $R_{h\ NP}$ = 36 nm at c_{NP} = 0.2 g L^{-1}. Here, the contribution of the free SiO_2 beads to the experimental $R_{vv}(q)$ and $D(q)$ is smaller but still significant. The characteristics of the internalization process for these two nanoparticles are summarized in Table 2.

The NP loading incorporation rate decreases compared to that of the smallest nanoparticle (see Table 1). For comparison, complete filling of the interior of the polymersome would correspond to x = 7 for $R_{h\ NP}$ = 36 nm and x = 3 for $R_{h\ NP}$ = 57 nm. In this context it should be mentioned that with a further increase of c_{NP} above the concentration necessary for the maximum filling of polymersomes no more changes of the systems are observed (no polymersomes rapture).

The two correlation spectroscopic techniques demonstrate that NPs reside inside the polymersomes but cannot provide information on the internal structure and in an indirect way (through the small size shrinkage) supports NP wrapping with polymeric bilayer. Alternatively, cryo-TEM imaging yields direct snapshots of a relatively small number of individual structures. The poor statistics can be, however, compensated by precise imaging with nanometer scale resolution. Figure 6 shows cryo-TEM images of the polymersomes containing SiO_2 NPs with two different sizes. Both types of particles are internalized into PDMS-*b*-PMOXA vesicles (for details see Figure S3 in Supporting Information). The incorporation mechanism derived from PCS and FCS results (*vide supra*) includes the complete engulfment and wrapping of NPs (see Figure S4 and S5 in Supporting Information). The number-average diameter of the wall thickness of the nanoparticles supported bilayer, as obtained by statistical analysis of several TEM micrographs, confirms the value of the membrane thickness of polymersomes (~16 nm). Albeit these two systems display very similar $R_{vv}(q)$ and $D(q)$, Figure 6a and 6b reveal size-dependent internalization mechanisms. SiO_2 NPs with $R_{h\ NP}$ = 14 nm were incorporated as clusters of

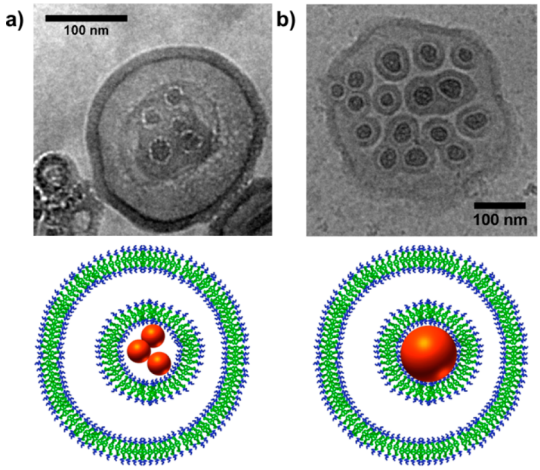

Figure 6. Cryo-TEM micrographs of incorporated SiO_2 nanoparticles into PDMS-*b*-PMOXA polymersomes. (a) Internalized groups of SiO_2 NPs with $R_{h\ NP}$ = 14 nm and (b) internalized single SiO_2 NPs with $R_{h\ NP}$ = 25 nm. The two schematic representations illustrate the different internalization mechanisms.

particles rather than single wrapped particles which appears to be the case for the larger SiO_2 nanoparticles ($R_{h\ NP}$ = 25 nm). For the larger sized particles the cryo-TEM preparations failed despite several repetitions. Only undefined collapsed objects together with the silica nanoparticles were found. This might be attributed to decreased vesicle stability after uptake of those larger silica particles.

Nanoparticle uptake by cells was very recently addressed by dissipative particle dynamics (DPD) simulation. It has shown that the mechanism of nanoparticle incorporation depends on the size, membrane tension, and nanoparticles concentration.[21] Small neighboring particles might cluster prior to internalization in order to reduce curvature energy of the membrane. An increase of the nanoparticle size would weaken the curvature-mediated interactions since large nanoparticle sizes reduce the perturbation of the membrane curvature. Thus the delicate balance of interactions renders different assemblies for small and large nanoparticles. These simulation results, although designed for cellular uptake of nanoparticles, bear strong resemblance with the cryo-TEM images in Figure 6 for the present artificial polymeric model system. The different properties of lipid and polymeric membranes such as in the thickness, however, render a direct comparison of nanoparticles ambiguous. Nevertheless, comparison is justified in view of the importance of surface curvature. Moreover, cryo-TEM images for the smaller silica nanoparticles ($R_{h\ NP}$ = 14 and 25 nm) were taken at about eight times higher concentration (but same ratio of NPs to polymersomes) than investigated by PCS and FCS. Because of the different solution compositions the quantitative comparison of the population of the incorporated particles observed in PCS and cryo-TEM is not straightforward.

CONCLUSIONS

The successful implementation of two complementary optical techniques: photon correlation and fluorescence correlation spectroscopies confirm strong adhesive interactions between polymersomes and nanoparticles through the selective probing of the involved species. Rapid internalization of the particles by polymersomes is observed only above a critical threshold particles concentration. The nanoparticles concentration affects the strength of the polymersomes/nanoparticles interactions and thus the number of incorporated particles can be tuned by a proper selection of their initial concentration. In addition to the effect of the concentration the phenomenon of nanosized particles incorporation by polymeric model membranes is found to be also strongly size-dependent as it is known from cellular systems. In this respect, the analogue behavior of the present artificial model system underlines the important role of physical parameters to trigger nanoparticles uptake even when all biofunctional molecules and/or supplementary energy are missing. Over a certain range of nanoparticles concentrations polymersomes were able to incorporate SiO_2 nanoparticles with sizes ranging from $R_{h\ NP}$ = 14 to 57 nm *via* an invagination and subsequent fission of the bilayer membrane.

Utilization of such artificial model systems and characterization methods has important implications for studies of physical and chemical aspects of transmembrane transport processes. Such investigations hardly implemented on natural membranes can be performed in simple model systems, yielding important insights on the parameters and pathways for nanoparticles uptake. The present experimental findings help create the missing phenomenology necessary for a detailed understanding of a phenomenon with great relevance in transmembrane transport.

METHODS

Materials. The poly(dimethylsiloxane)-*block*-poly(2-methyloxazoline) copolymer ($PDMS_{68}$-*b*-$PMOXA_{11}$), where the numbers refer to the number-average degree of polymerization, with piperazyl functionality at the hydrophilic end was synthetized as described elsewhere.[52] Silica nanoparticles (SiO_2 NPs) with $R_{h\ NP}$ = (14 ± 1), (25 ± 2), (36 ± 2), and (57 ± 2) nm, respectively, were ordered from Kisker Biotech GmbH & Co. The fluorescent dye Nile Blue (Acros Organics) was used without further purification. Ethanol (≥99.5%) was ordered form Sigma Aldrich. All experiments were performed in aqueous solutions (Millipore, Milli-Q water with a conductivity < 18.2 MΩ·cm) without any additives. The zeta-potentials of silica nanoparticles as well as polymersomes in aqueous solutions were determined by MALVERN Zetasizer Nano Z (see Supporting Information).

Sample Preparation. Polymersomes of PDMS-*b*-PMOXA were prepared using a film rehydratation method followed by extrusion process as described in the literature.[53] The copolymer was placed in a small (10 mL) round-bottom flask and solved in ethanol. Ethanol was evaporated using the rotary evaporator under reduced pressure at a temperature of T = 40 °C. The final thin polymer film that formed on the wall of the flask was dried under vacuum for 1 h at room temperature. Ultrapure water (Millipore, Milli-Q water with a conductivity < 18.2 MΩ·cm) was added and the sample was stirred overnight using a magnetic stirrer. Subsequently, the resulting polymersome suspension was extruded 11 times through a polycarbonate membrane (Avestin, 0.2 μm pore size) to homogenize the final vesicle size of $R_{h\ P} \approx$ 110 nm. The Nile Blue labeling of polymersomes was achieved by the addition of the dye to the initial copolymer/ethanol solution. Samples for size-dependent nanoparticles incorporation experiments were prepared one day prior the measurement by the addition of SiO_2 nanoparticles of desired size to the dilute aqueous vesicle suspensions (c_P = 4.5 × 10^{-2} g L^{-1}). Samples with different nanoparticle concentrations (c_{NP} = 0.05, 0.1, 0.15, and 0.2 g L^{-1}) were prepared according to the same procedure by varying the final nanoparticle concentrations in the mixture.

Photon Correlation Spectroscopy (PCS). Static (SLS) and dynamic light scattering (DLS) experiments were performed on a commercially available instrument from ALV GmbH consisting of a goniometer and an ALV-5004 multiple-tau full-digital correlator (320 channels), which allows measurements of the intensity autocorrelation function $g(q, t)$ over a time range $10^7 \leq t \leq 10^3$ s and an angular range from 20° to 150°. A He–Ne laser (Uniphase with a single mode intensity of 25 mW operating at a laser wavelength of λ_0 = 632.8 nm) was used as the light source. All measurements were carried out at temperature T = 20 °C. Dust-free solutions for light scattering experiments were obtained by filtration through PTFE membrane filters with a pore size of 5 μm (Millipore, Millex-LS) into silica glass light scattering cuvettes (Hellma, inner diameter ∅ = 10 mm), which were cleaned prior to the procedure with acetone in a Thurmont-apparatus. The theoretical details of the experiments are given elsewhere.[54] DLS data evaluation was performed by using the stretched exponential Kohlrausch–Williams–Watts (KWW) function.[55,56] This method assumed that for single but nonexponential decay, the computed (from $g(q, t)$) relaxation function $C(q, t)$ can be represented by

$$C(q, t) = \exp[-(t/\tau_{KWW}{}^{*}(q))^{\beta_{KWW}}] \quad (1)$$

where τ_{KWW} is the relaxation time and β_{KWW} is the shape parameter ranging as $0 \leq \beta_{KWW} \leq 1$ characterizing the distribution of relaxation times. The form factor description for polymersomes in solution and its application to detect refractive index changes in the interior of polymersomes can be found in the literature.[49,25]

Fluorescence Correlation Spectroscopy (FCS). The experiments were performed on a semicommercial setup based on an inverted microscope IX70 (Olympus, Japan) combined with the FluoView300 confocal laser scanning unit (Olympus, Japan) and an FCS upgrade kit (PicoQuant, Germany). The latter is fiber coupled to the FluoView300 and has two detection channels separated by a dichroic mirror and possessing separate emission filters and a Single Photon Avalanche Diode (τ-SPAD) detectors (PicoQuant, Germany). A TimeHarp 200 time-correlated single-photon counting card in combination with the software package SymPhoTime (both PicoQuant, Germany) is used for data acquisition and analysis. An Olympus UPLSAPO 60XW, 60×/NA 1.2 water immersion objective was used in all studies. The fluorescently labeled silica nanoparticles were excited by an argon-ion laser at λ = 488 nm and their emission was detected after filtering with a BP525/50 band-pass filter. The Nile Blue labeled polymersomes were excited by a helium–neon laser at λ = 633 nm and the emission was detected after filtering through a LP635R long-pass filter. An eight-well, polystyrene-chambered cover glass (Laboratory-Tek, Nalge Nunc International) was used as sample cell. For each sample a series of 10 measurements with a total duration of 5 min were performed. The fluctuations of the fluorescence intensity $F(t)$ caused by the diffusion of the silica nanoparticles or the

polymersomes through the confocal detection volume were separately monitored in the respective detection channels and evaluated in terms of an autocorrelation function $G(t) = \langle F(t')F(t+t')\rangle/\langle F(t')\rangle^2$.

As has been shown theoretically for an ensemble of m different types of freely diffusing fluorescence species, $G(t)$ has the following analytical form:[57]

$$G(t) = 1 + \frac{1}{N}\sum_{i=1}^{m} \frac{f_i}{\left[1+\frac{t}{t_{Di}}\right]\sqrt{1+\frac{t}{S^2 t_{Di}}}} \quad (2)$$

Here, N is the average number of diffusing fluorescence species in the observation volume, τ_{Di} is the diffusion time of the ith species, f_i is the fraction of component i, and S is the so-called structure parameter, $S = z_0/r_0$, where z_0 and r_0 represent the axial and radial dimensions of the confocal volume V, respectively. Furthermore the diffusion time, τ_{Di}, is related to the respective diffusion coefficient, D_i, through $D_i = (r_0^2 + R_{h,i}^2)/4\tau_i$, where $R_{h,i}$ is the hydrodynamic radius, which is also connected to the diffusion coefficient through the Stokes−Einstein-relationship. Thus a fit of an experimental autocorrelation function with eq 1 provides, the overall concentration of the fluorescent species $c = N/V$, as well as the hydrodynamic radius $R_{h,i}$ and the number fraction f_i of each diffusing component.

However, as the size of the observation volume V depends strongly on the specific characteristics of the optical setup and the refractive index of the studied samples a suitable calibration, relying on the measurement of the characteristic diffusion time of a fluorescent tracer with known diffusion coefficient, is needed. Here we used Alexa Fluor 488 and Alexa Fluor 647 (Invitrogen), for calibration of the two detection channels, respectively.

Cryogenic Transmission Electron Microscopy (cryo-TEM). TEM measurements were performed using a Tecnai F20 transmission electron microscope from FEI Co. with integrated electron energy-loss spectrometer, operated at a 200 kV acceleration voltage. The aqueous solution was dropped onto a quantifoil (R) grid followed by blotting off of the excess amount with filter paper. Subsequently, the sample was frozen in liquid ethane at $T = -178$ °C and transferred to the TEM instrument for further inspection.

Conflict of Interest: The authors declare no competing financial interest.

Acknowledgment. This work was supported by the Max Planck Graduate Center (MPGC) of the Max Planck Society and the Johannes Gutenberg University Mainz. The authors gratefully thank W. Meier, S. Egli, and D. Wu (University of Basel) for the synthesis of PDMS-*b*-PMOXA copolymer.

Supporting Information Available: Additional figures of the absolute Rayleigh intensity $R_{vv}(q)$ of SiO_2 NPs with different sizes at $c_{NP} = 0.2$ g L^{-1}; $R_{vv}(q)$ of empty polymersomes and SiO_2 ($R_{h\ NP} = 25$ nm)/polymersome systems at three different concentration of particles; cryo-TEM micrograph of SiO_2/polymersome systems recorded on sample frozen 6 min after the addition of NPs as well as additional cryo-TEM micrographs; tables of characteristics of polymersomes in the absence and presence of SiO_2 NPs ($R_{h\ NP} = 25$ nm); zeta-potential of all nanoparticles and polymersomes; details of PCS data evaluation. This material is available free of charge *via* the Internet at http://pubs.acs.org.

REFERENCES AND NOTES

1. Chan, Y. H. M.; Boxer, S. G. Model Membrane Systems and Their Applications. *Curr. Opin. Chem. Biol.* **2007**, *11*, 581–587.
2. Knoll, W.; Köper, I.; Naumann, R.; Sinner, E. K. Tethered Bimolecular Lipid Membranes—A Novel Model Membrane Platform. *Electrochim. Acta* **2008**, *53*, 6680–6689.
3. Zepik, H.; Walde, P.; Kostoryz, E.; Yourtee, D. Lipid Vesicles as Membrane Models for Toxicological Assessment of Xenobiotics. *Crit. Rev. Toxicol.* **2008**, *38*, 1–11.
4. Ringsdorf, H.; Schlarb, B.; Venzmer, J. Molecular Architecture and Function of Polymeric Oriented Systems: Models for the Study of Organization, Surface Recognition, and Dynamics of Biomembranes. *Angew. Chem., Int. Ed.* **1988**, *27*, 113–158.
5. Naumann, R.; Schiller, S. M.; Giess, F.; Grohe, B.; Hartman, K. B.; Kärcher, I.; Köper, I.; Lübben, J.; Vasilev, K.; Knoll, W. Tethered Lipid Bilayers on Ultraflat Gold Surfaces. *Langmuir* **2003**, *19*, 5435–5443.
6. Sackmann, E. Supported Membranes: Scientific and Practical Applications. *Science* **1996**, *271*, 43–48.
7. Tanaka, M.; Sackmann, E. Polymer-Supported Membranes as Models of the Cell Surface. *Nature* **2005**, *437*, 656–663.
8. Belegrinou, S.; Dorn, J.; Kreiter, M.; Kita-Tokarczyk, K.; Sinner, E. K.; Meier, W. Biomimetic Supported Membranes from Amphiphilic Block Copolymers. *Soft Matter* **2009**, *6*, 179–186.
9. Discher, D. E.; Eisenberg, A. Polymer Vesicles. *Science* **2002**, *297*, 967.
10. Tanner, P.; Egli, S.; Balasubramanian, V.; Onaca, O.; Palivan, C. G.; Meier, W. Can Polymeric Vesicles that Confine Enzymatic Reactions Act as Simplified Organelles? *FEBS Lett.* **2011**, *585*, 1699–1706.
11. Marguet, M.; Edembe, L.; Lecommandoux, S. Polymersomes in Polymersomes: Multiple Loading and Permeability Control. *Angew. Chem., Int. Ed.* **2012**, *124*, 1199–1202.
12. Antonietti, M.; Förster, S. Vesicles and Liposomes: A Self-Assembly Principle Beyond Lipids. *Adv. Mater.* **2003**, *15*, 1323–1333.
13. Conner, S. D.; Schmid, S. L. Regulated Portals of Entry into the Cell. *Nature* **2003**, *422*, 37–44.
14. Liu, J.; Sun, Y.; Oster, G. F.; Drubin, D. G. Mechanochemical Crosstalk During Endocytic Vesicle Formation. *Curr. Opin. Cell Biol.* **2010**, *22*, 36–43.
15. Marsh, M.; McMahon, H. The Structural Era of Endocytosis. *Science* **1999**, *285*, 215.
16. Illya, G.; Lipowsky, R.; Shillcock, J. Effect of Chain Length and Asymmetry on Material Properties of Bilayer Membranes. *J. Chem. Phys.* **2005**, *122*, 244901.
17. Fošnarič, M.; Iglič, A.; Kroll, D. M.; May, S. Monte Carlo Simulations of Complex Formation between a Mixed Fluid Vesicle and a Charged Colloid. *J. Chem. Phys.* **2009**, *131*, 105103.
18. Dietrich, C.; Angelova, M.; Pouligny, B. Adhesion of Latex Spheres to Giant Phospholipid Vesicles: Statics and Dynamics. *J. Phys. II* **1997**, *7*, 1651–1682.
19. Deserno, M.; Gelbart, W. M. Adhesion and Wrapping in Colloid-Vesicle Complexes. *J. Phys. Chem. B* **2002**, *106*, 5543–5552.
20. Deserno, M.; Bickel, T. Wrapping of a Spherical Colloid by a Fluid Membrane. *Europhys. Lett.* **2003**, *62*, 767.
21. Yue, T.; Zhang, X. Cooperative Effect in Receptor-Mediated Endocytosis of Multiple Nanoparticles. *ACS Nano* **2012**, *6*, 3196–3205.
22. Smith, K. A.; Jasnow, D.; Balazs, A. C. Designing Synthetic Vesicles that Engulf Nanoscopic Particles. *J. Chem. Phys.* **2007**, *127*, 084703.
23. Lipowsky, R.; Döbereiner, H. G. Vesicles in Contact with Nanoparticles and Colloids. *Europhys. Lett.* **1998**, *43*, 219.
24. Le Bihan, O.; Bonnafous, P.; Marak, L.; Bickel, T.; Trépout, S.; Mornet, S.; De Haas, F.; Talbot, H.; Taveau, J. C.; Lambert, O. Cryo-Electron Tomography of Nanoparticle Transmigration into Liposome. *J Struct Biol* **2009**, *168*, 419–425.
25. Jaskiewicz, K.; Larsen, A.; Lieberwirth, I.; Koynov, K.; Meier, W.; Fytas, G.; Kroeger, A.; Landfester, K. Probing Bioinspired Transport of Nanoparticles into Polymersomes. *Angew. Chem., Int. Ed.* **2012**, *51*, 4613–4617.
26. Michalet, X.; Pinaud, F.; Bentolila, L.; Tsay, J.; Doose, S.; Li, J.; Sundaresan, G.; Wu, A.; Gambhir, S.; Weiss, S. Quantum Dots for Live Cells, *in Vivo* Imaging, and Diagnostics. *Science* **2005**, *307*, 538.
27. Cao, Y. W. C.; Jin, R.; Mirkin, C. A. Nanoparticles with Raman Spectroscopic Fingerprints for DNA and RNA Detection. *Science* **2002**, *297*, 1536.
28. Nel, A. E.; Mädler, L.; Velegol, D.; Xia, T.; Hoek, E. M. V.; Somasundaran, P.; Klaessig, F.; Castranova, V.; Thompson,

M. Understanding Biophysicochemical Interactions at the Nano−Bio Interface. *Nat. Mater.* **2009**, *8*, 543–557.
29. Yan, Y.; Such, G. K.; Johnston, A. P. R.; Best, J. P.; Caruso, F. Engineering Particles for Therapeutic Delivery: Prospects and Challenges. *ACS Nano* **2012**, *6*, 3663–3669.
30. Merrifield, C. J.; Feldman, M. E.; Wan, L.; Almers, W. Imaging Actin and Dynamin Recruitment During Invagination of Single Clathrin-Coated Pits. *Nat. Cell Biol.* **2002**, *4*, 691–698.
31. Jonsdottir, G. A.; Li, R. Dynamics of Yeast Myosin I: Evidence for a Possible Role in Scission of Endocytic Vesicles. *Curr. Biol.* **2004**, *14*, 1604–1609.
32. Rothen-Rutishauser, B. M.; Schürch, S.; Haenni, B.; Kapp, N.; Gehr, P. Interaction of Fine Particles and Nanoparticles with Red Blood Cells Visualized with Advanced Microscopic Techniques. *Environ. Sci. Technol.* **2006**, *40*, 4353–4359.
33. Liu, C.; Zhen, X.; Wang, X.; Wu, W.; Jiang, X. Cellular Entry Fashion of Hollow Milk Protein Spheres. *Soft Matter* **2011**, *7*, 11526–11534.
34. Sharma, A.; Sharma, U. S. Liposomes in Drug Delivery: Progress and Limitations. *Int. J. Pharm.* **1997**, *154*, 123–140.
35. Schulz, M.; Olubummo, A.; Binder, W. H. Beyond the Lipid-Bilayer: Interaction of Polymers and Nanoparticles with Membranes. *Soft Matter* **2012**, *8*, 4849–4864.
36. Batzri, S.; Korn, E. D. Single Bilayer Liposomes Prepared without Sonication. *BBA-Biomembranes* **1973**, *298*, 1015–1019.
37. Le Meins, J. F.; Sandre, O.; Lecommandoux, S. Recent Trends in the Tuning of Polymersomes' Membrane Properties. *Eur. Phys. J. E* **2011**, *34*, 1–17.
38. Bermudez, H.; Brannan, A. K.; Hammer, D. A.; Bates, F. S.; Discher, D. E. Molecular Weight Dependence of Polymersome Membrane Structure, Elasticity, and Stability. *Macromolecules* **2002**, *35*, 8203–8208.
39. Blok, M.; Van der Neut-Kok, E.; Van Deenen, L.; De Gier, J. The Effect of Chain Length and Lipid Phase Transitions on the Selective Permeability Properties of Liposomes. *BBA-Biomembranes* **1975**, *406*, 187–196.
40. Chen, R.; Pearce, D. J. G.; Fortuna, S.; Cheung, D. L.; Bon, S. A. F. Polymer Vesicles with a Colloidal Armor of Nanoparticles. *J. Am. Chem. Soc.* **2011**, *133*, 2151–2153.
41. Letchford, K.; Burt, H. A Review of the Formation and Classification of Amphiphilic Block Copolymer Nanoparticulate Structures: Micelles, Nanospheres, Nanocapsules and Polymersomes. *Eur. J. Pharm. Sci.* **2007**, *65*, 259–269.
42. LoPresti, C.; Lomas, H.; Massignani, M.; Smart, T.; Battaglia, G. Polymersomes: Nature Inspired Nanometer Sized Compartments. *J. Mater. Chem.* **2009**, *19*, 3576–3590.
43. Chithrani, B. D.; Ghazani, A. A.; Chan, W. C. W. Determining the Size and Shape Dependence of Gold Nanoparticle Uptake into Mammalian Cells. *Nano Lett.* **2006**, *6*, 662–668.
44. Chithrani, B. D.; Chan, W. C. W. Elucidating the Mechanism of Cellular Uptake and Removal of Protein-Coated Gold Nanoparticles of Different Sizes and Sapes. *Nano Lett.* **2007**, *7*, 1542–1550.
45. Jin, H.; Heller, D. A.; Sharma, R.; Strano, M. S. Size-Dependent Cellular Uptake and Expulsion of Single-Walled Carbon Nanotubes: Single Particle Tracking and a Generic Uptake Model for Nanoparticles. *ACS Nano* **2009**, *3*, 149–158.
46. Andersson, P. O.; Lejon, C.; Ekstrand-Hammarström, B.; Akfur, C.; Ahlinder, L.; Bucht, A.; Österlund, L. Polymorph- and Size-Dependent Uptake and Toxicity of TiO_2 Nanoparticles in Living Lung Epithelial Cells. *Small* **2011**, *7*, 514–523.
47. Jiang, W.; Kim, B. Y. S.; Rutka, J. T.; Chan, W. C. W. Nanoparticle-Mediated Cellular Response Is Size-Dependent. *Nat. Nanotechnol.* **2008**, *3*, 145–150.
48. Zhang, S.; Li, J.; Lykotrafitis, G.; Bao, G.; Suresh, S. Size-Dependent Endocytosis of Nanoparticles. *Adv. Mater.* **2009**, *21*, 419–424.
49. Hallett, F.; Watton, J.; Krygsman, P. Vesicle Sizing: Number Distributions by Dynamic Light Scattering. *Biophys. J.* **1991**, *59*, 357–362.
50. Mornet, S.; Lambert, O.; Duguet, E.; Brisson, A. The Formation of Supported Lipid Bilayers on Silica Nanoparticles Revealed by Cryoelectron Microscopy. *Nano Lett.* **2005** *5*, 281–285.
51. Peterlin, P.; Arrigler, V.; Haleva, E.; Diamant, H. Law of Corresponding States for Osmotic Swelling of Vesicles. *Soft Matter* **2012**, *8*, 2185–2193.
52. Egli, S.; Nussbaumer, M. G.; Balasubramanian, V.; Chami, M.; Bruns, N.; Palivan, C.; Meier, W. Biocompatible Functionalization of Polymersome Surfaces: A New Approach to Surface Immobilization and Cell Targeting Using Polymersomes. *J. Am. Chem. Soc.* **2011**, *133*, 4476–4483.
53. Olson, F.; Hunt, C.; Szoka, F.; Vail, W.; Papahadjopoulos, D. Preparation of Liposomes of Defined Size Distribution by Extrusion through Polycarbonate Membranes. *BBA-Biomembranes* **1979**, *557*, 9–23.
54. Kroeger, A.; Deimede, V.; Belack, J.; Lieberwirth, I.; Fytas, G.; Wegner, G. Equilibrium Length and Shape of Rodlike Polyelectrolyte Micelles in Dilute Aqueous Solutions. *Macromolecules* **2007**, *40*, 105–115.
55. Berberan-Santos, M.; Bodunov, E.; Valeur, B. Mathematical Functions for the Analysis of Luminescence Decays with Underlying Distributions 1. Kohlrausch Decay Function (Stretched Exponential). *Chem. Phys.* **2005**, *315*, 171–182.
56. Brown, W. *Dynamic Light Scattering: The Method and Some Applications*; Oxford University Press: Oxford, 1993.
57. Rigler, R.; Elson, E. *Fluorescence Correlation Spectroscopy: Theory and Applications*; Springer Verlag: Heidelberg, Germany, 2001.